ISSN 0021-8944, Journal of Applied Mechanics and Technical Physics, 2020, Vol. 61, No. 5, pp. 717–726. © Pleiades Publishing, Ltd., 2020.
Russian Text © P.A. Polivanov, D.V. Khotyanovsky, A.I. Kutepova, A.A. Sidorenko.

INVESTIGATION OF VARIOUS APPROACHES TO THE SIMULATION OF LAMINAR–TURBULENT TRANSITION IN COMPRESSIBLE SEPARATED FLOWS

P. A. Polivanov*, D. V. Khotyanovsky, A. I. Kutepova, and A. A. Sidorenko

UDC 533

Abstract: The interaction of a laminar boundary layer with a shock wave at a Mach number M = 1.43 is studied by numerical simulation. The results obtained by direct numerical simulation are compared with the results of calculations using the Reynolds-averaged Navier–Stokes (RANS) equations supplemented with different turbulence models describing laminar–turbulent transition. The possibility of determining the position of the flow turbulence zone based on linear stability theory and the e^N-method is estimated. Comparison of the numerical simulation with experimental data shows that engineering RANS methods can be used to study supersonic flows in which transition to turbulence occurs in regions of shock wave–boundary layer interaction.

Keywords: boundary layer, shock wave, laminar–turbulent transition, flow separation, direct numerical simulation, Reynolds equations, linear stability theory.

DOI: 10.1134/S0021894420050053

INTRODUCTION

The interaction of a shock wave with a boundary layer leads to the formation of rather complex flow which is often encountered in the gas-dynamic design of aircraft and their elements, turbomachinery blades, air intakes, aircraft engine nozzles, etc. [1]. Shock wave–boundary layer interaction causes flow separation and generates flow unsteadiness, which can manifest itself both locally and globally. In the first case, additional variable dynamic and thermal loads on the structure arise, and in the second case, quasiperiodic fluctuations of the entire flow occur, as in the case of, e.g., transonic wing buffet. Due to the importance for practical applications, this phenomenon has been actively studied over the past 50 years [2], and currently there are several fairly detailed reviews (see, e.g., [3, 4]) of research on the interaction of shock waves with a turbulent boundary layer, in which much attention is paid to the mechanisms underlying the onset of unsteadiness of separated flows [5, 6].

Flow fluctuations during shock wave–boundary layer interaction are characterized by a wide frequency range, including frequencies characteristic of the incoming boundary layer and frequencies one to two orders of magnitude lower. The study of the low-frequency range of fluctuations is of greatest interest and involves the greatest difficulties

Khristianovich Institute of Theoretical and Applied Mechanics, Siberian Branch, Russian Academy of Sciences, Novosibirsk, 630090 Russia; *polivanov@itam.nsc.ru; dima@itam.nsc.ru; a.kutepova@g.nsu.ru; sindr@itam.nsc.ru. Translated from Prikladnaya Mekhanika i Tekhnicheskaya Fizika, Vol. 61, No. 5, pp. 40–51, September–October, 2020. Original article submitted June 26, 2020; revision submitted June 26, 2020; accepted for publication July 27, 2020.

*Corresponding author.

in numerical simulation [7]. The causes of the occurrence of low-frequency fluctuations have been investigated in detail in theoretical, numerical, and experimental studies, which are analyzed, e.g., in [8]. The results of the studies suggest that fluctuations of the interaction zone can be caused by disturbances present in the incoming boundary layer, as well as by some large-scale instability characteristic of separated flow. As a rule, in all turbulent separated flows caused by a shock wave, both mechanisms are present; however, in the case of flows with developed separation, the second mechanism dominates.

Laminar flows have recently been used more widely due to the need for aerodynamic improvement of aircraft and turbojet engines. This leads to the need to study the interaction of shock waves with a laminar boundary layer, which is greatly influenced by an unfavorable pressure gradient that arises at the shock wave. The resulting extended separation zones and an additional aerodynamic drag can reduce the advantages of flow laminarization. In this connection, a large number of studies have recently been performed to study the interaction of shock waves with laminar and transitional boundary layers at supersonic speeds and the control of these flows [2]. Calculations of such flows require methods that take into account laminar–turbulent transition [9].

Flow calculation methods based on Reynolds-averaged Navier–Stokes (RANS) equations are often used for numerical simulation of a wide range of applied problems. A review of papers devoted to the modeling of shock wave–boundary layer interaction (SWBLI) using RANS methods for 2D and 3D interactions is given in [10], where turbulence models from algebraic to full Reynolds stress equations are considered and it is noted that these models poorly predict the magnitude of the heat flux and the skin friction coefficient. In this case, the largest difference between simulation results and experimental data are observed in the case of strong interaction with developed separation zones.

Various RANS codes for modeling problems of the interaction of a shock wave with a turbulent boundary layer for moderate Mach numbers (M = 1.3–1.7) were considered in the unsteady effects of shock wave induced separation (UFAST) project [7]. It has been found that the parameters of the boundary layer before and after the interaction are generally well reproduced in the calculation, but the size of the separation zone differs from that obtained in experiment and depends on the turbulence model used. In addition, it has been shown that RANS methods do not predict the characteristics of natural low-frequency oscillations of the separation zone.

Due to the limited capabilities of the RANS method used to model flows with SWBLI, studies have been performed using large-eddy simulation (LES) [11, 12] and direct numerical simulation (DNS) [13, 14]. It has been shown [13–15] that the interaction of shocks with a turbulent boundary layer can be investigated by eddy-resolving numerical simulation. In particular, the results of calculations using LES and the subgrid turbulence model describe the global structure of the interaction of an oblique shock wave with a boundary layer [13]. Direct numerical simulation of a supersonic turbulent boundary layer with a resolution of all eddy flow scales is now possible only for relatively small Reynolds numbers [14, 15]. Direct numerical simulation of the transition to turbulence in the boundary layer on a flat plate at a Mach number M = 3 was performed in [16]; direct numerical simulation of the transition on a plate and at a compression corner at M = 5.3 was carried out in [17]; transition in a boundary layer at M = 2 and 6 was simulated in [18, 19]. Analysis of these and other works shows that LES and DNS are capable of predicting all major physical phenomena typical of flows with SWBLI; however, the current level of development of computer technology does not allow these methods to be used to solve practical problems.

The aim of this work is to compare the results of RANS simulation using semi-empirical models of laminar–turbulent transition with the results of DNS of shock wave–boundary layer interaction at a moderate supersonic Mach number (M = 1.43).

1. FORMULATION OF THE PROBLEM FOR NUMERICAL SIMULATION

The calculations were carried out using two approaches: solution of the Reynolds-averaged Navier–Stokes equations and DNS with a resolution of the eddy structure of the flow based on the solution of the unsteady Navier–Stokes equations. The geometry of the computational domain and the flow parameters were the same as in the experiments performed on the T-325 wind tunnel at the Institute of Theoretical and Applied Mechanics of the Siberian Branch of the Russian Academy of Sciences (ITAM SB RAS) [20]. The interaction of a laminar boundary layer on a flat plate with an incident oblique shock wave is considered. In all calculations, the flow Mach number

is M = 1.43, the stagnation pressure $P_0 = 0.55 \cdot 10^5$ Pa, and the stagnation temperature $T_0 = 293$ K. In RANS calculations, the zero heat flux boundary condition on the plate wall was used, and in DNS, the plate temperature T_w was assumed to be constant and equal to the surface temperature in laminar flow around a heat-insulated plate. The angle of attack of the shock wave generator is 3°, and the point of intersection of the incident shock wave with the plate (in the inviscid flow approximation) is located at a distance of 111 mm from the leading edge of the plate.

RANS simulation was carried out using ANSYS Fluent software. The integration of the Navier–Stokes equations was performed using a density-based solver, an implicit scheme of the second order in space and the advection upstream splitting method (AUSM) for splitting convective flows. In the calculations, we used turbulence models that take into account laminar–turbulent transition: $\varkappa$–ω–γ–Re_θ, $\varkappa$–ω–γ, and $\varkappa_L$–$\varkappa_T$–ω (Re_θ is the Reynolds number based on the momentum thickness). For these models, intermittency or laminar kinetic energy at the input were set equal to zero. In addition, we used the ($\varkappa$–ω)-SST model, which assumed that the position of the turbulence onset point corresponds to zero turbulent viscosity in the region of laminar flow. The turbulence parameters at the input boundary were the characteristic hydraulic diameter and the level of velocity fluctuations, which were set equal to 5 mm and 0.1%, respectively [21].

RANS simulation was implemented for a 2D problem in accordance with the experimental geometry [22]. A block-structured grid containing 110 000 cells was used. Not less than 50 cells fell into the boundary layer, and the grid refinement in the boundary layer satisfied the condition $y^+ < 1$. In the calculation, a shock was generated by the geometry of the computational domain.

In the DNS, the development of disturbances in the incoming boundary layer and separated flow was considered. The three-dimensional computational domain was shaped like a parallelepiped whose lower face coincided with the plane of the plate. The dimensions of the domain along the X, Y, and Z coordinates are equal to 168.0, 10.0, and 7.2 mm, respectively. The left edge of the computational domain is at a distance $X = 58$ mm from the leading edge. The boundary condition at the upper boundary of the computational domain corresponded to the longitudinal distribution of the inviscid flow parameters when the oblique shock wave resulting from the flow turning by an angle of 3° passed through this boundary. In this case, the rarefaction wave propagating from the trailing edge of the wedge was not modeled.

The calculations were carried out using the CFS3D computer codes developed at the ITAM SB RAS. The numerical simulation procedure includes several steps. The first step is a two-dimensional calculation of the basic laminar flow for which the most unstable discrete disturbance mode is determined by solving the linear stability problem. In the second step, the spatial development of this disturbance in the boundary layer is calculated by solving the full three-dimensional Navier–Stokes equations. As a result, in the problem under study, the basic flow at the input boundary is superimposed with two unstable disturbances of a Tollmien–Schlichting wave with a frequency $f = 25.1$ kHz, which propagate at angles $\chi = \pm 46°$ to the direction of the basic flow in the transverse direction z. The width of the computational domain corresponded to one wavelength in the transverse direction, and periodic boundary conditions along the z coordinate were used. Also, in the calculations, we used a rectangular structured computational grid with $N_x = 1000$, $N_y = 200$, and $N_z = 80$ cells along the X, Y, and Z coordinate axes. The initial amplitude of the disturbance wave determined from the magnitude of fluctuations of the longitudinal velocity component in the input section was 0.1% of the velocity in the undisturbed flow. To obtain averaged data after the establishment of the flow, the calculation was continued for six periods of the unstable mode. Note that the quality of the grid did not allow modeling the entire characteristic frequency range in the region of turbulent flow. Therefore, the data obtained after the transition of the boundary layer to turbulence can be used mainly for qualitative analysis.

Locally parallel linear theory for calculating the disturbance growth rates in gradientless boundary layers has been verified many times and its use is not difficult. To evaluate the validity of modeling using linear stability theory (LST) in the separation zone, the obtained results were compared with the results of DNS. The growth of the disturbance amplitude using linear theory was calculated using the averaged flow parameters obtained by DNS. Data on the growth in the amplitude of disturbances in the DNS were obtained using pressure oscillograms, the skin friction on the plate surface, and the Fourier integral for the frequency of the introduced disturbance.

Since experimental parameters are modeled, the data are presented in dimensional form, making it possible to simplify the comparison with experiment and eliminate the errors due to the use of normalizing parameters that depend on the accuracy of solution of the problem (e.g., the size of the separation zone).

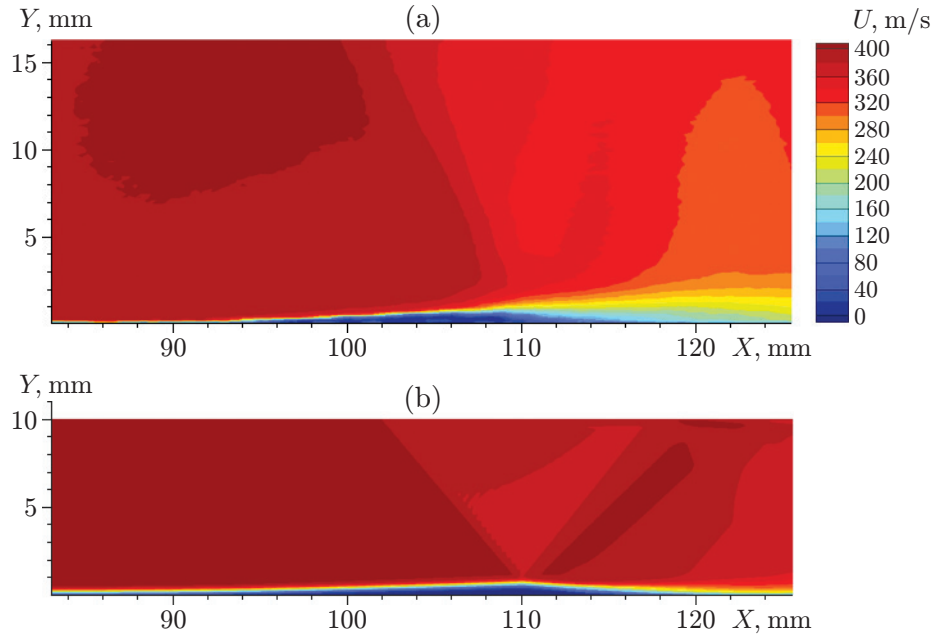

Fig. 1. Velocity distributions in the (X, Y) plane obtained in the experiment (a) and by DNS simulation (b).

2. CALCULATION RESULTS

In Fig. 1, which shows the velocity distributions obtained in the experiment [20] and by DNS simulation, one can clearly see a developed laminar separated flow in the region $X = 94$–112 mm. The separation is caused by an unfavorable pressure gradient that arises due to the impact of the incident oblique shock intersecting the plate at the point $X = 111$ mm. In the vicinity of this point, the pressure increases sharply and flow transition to turbulence occurs due to a significant increase in the amplitude of disturbances. The flow displacement in the laminar bubble zone gives rise to compression waves, which attenuate the main incident shock. Note that the inertia of the tracers used in the PIV method leads to the smearing of high velocity gradients in space, as is the case in the shock-wave region (see Fig. 1a). The DNS results (see Fig. 1b) are close to the results of the experiment.

It is also seen in Fig. 1 that the experimental and calculated angles of the incident shock are different. This can be explained by two reasons. The first is that in the experiment, the boundary-layer displacement thickness in the separation zone is greater. This leads to the formation of a more intense fan of compression waves propagating from the separation zone, resulting in a decrease in the local Mach number ahead of the incident shock wave and a decrease in the shock angle. The second reason is that the Mach number is smaller than the real Mach number obtained from measurements of the static pressure in the freestream flow ahead of the interaction zone in the experiment. This may be due to a decrease in the Mach number in the presence of weak disturbances occurring at the junction of the nozzle with the test section in the experiment.

The main differences are observed in the wake region. As a result of flow transition to turbulence, the thickness of the turbulent boundary layer is smaller in DNS simulation than in the experiment. The smaller displacement thickness in the wake in the calculation leads to the formation of a stronger rarefaction wave upon shock reflection from the boundary layer, resulting in a lower unfavorable pressure gradient in the calculation than in the experiment. This may explain the more rapid increase in the separation bubble in the experiment compared with the calculation.

Results of DNS and RANS simulations using the $\varkappa$–ω–γ–Re_θ turbulence models are shown in Fig. 2. It is seen that the sizes of the separation zone are in good agreement, as follows from the coincidence of the pressure distributions in this region. However, in the wake region, the pressure in the RANS calculation increases more rapidly for two reasons: (1) different rates of increase in the displacement thickness in the turbulent wake, which can be explained by the complexity of modeling the turbulent wake using semiempirical RANS methods; (2) the effect of the relatively low height of the computational domain used in the DNS, due to which compression

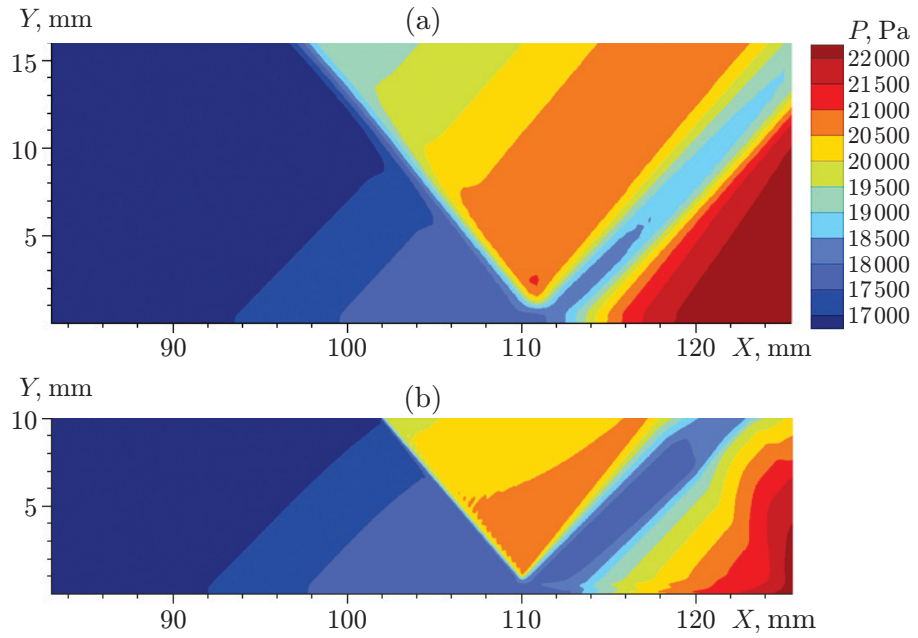

Fig. 2. Static pressure fields obtained by RANS simulation (a) and DNS simulation (b).

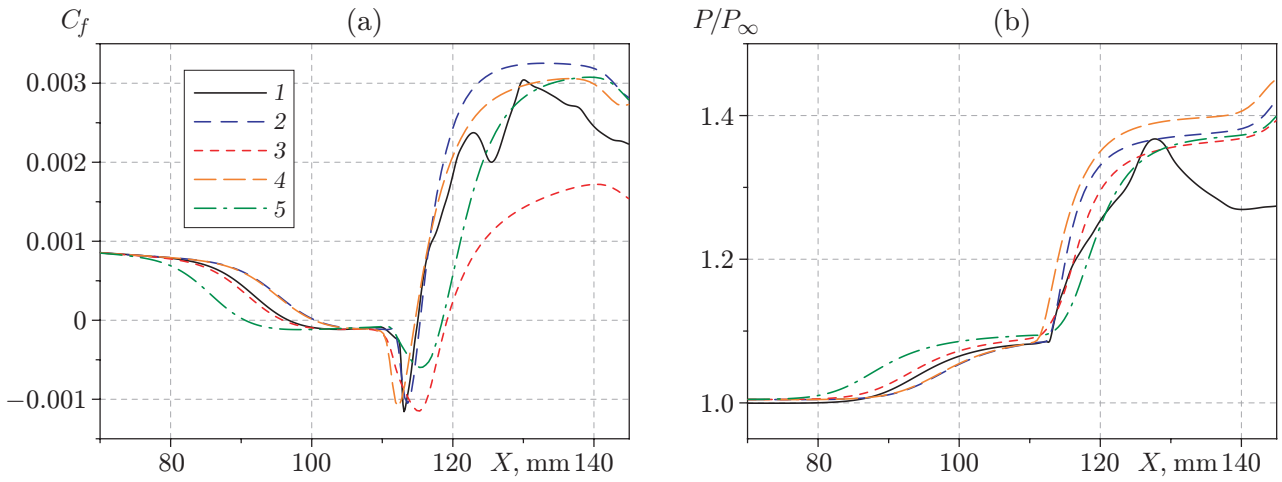

Fig. 3. Distributions of wall skin friction (a) and pressure (b) obtained by DNS (curve *1*) and RANS simulation for the ($\varkappa$–ω–γ–Re_θ) model (curve *2*), the ($\varkappa_T$–$\varkappa_L$–ω) model (curve *3*), the ($\varkappa$–ω–γ) model (curve *4*), and the ($\varkappa$–ω)-SST model at $X_t = 111$ mm (curve *5*).

waves reach the upper boundary of the computational zone in the shock formation region (see Fig. 2b), and the incident shock wave in the DNS simulation is specified at the upper boundary neglecting the pressure change in compression waves. As a result, the pressure distributions behind the incident shock obtained by DNS and RANS simulations differ only slightly. However, this effect is rather weak and the pressure distribution behind the shock changes insignificantly. Therefore, further, when comparing the results of DNS and RANS calculations, the data obtained by DNS are considered basic.

Figure 3 shows the skin friction and pressure distributions obtained using different computational methods. It is seen that they are in fairly good qualitative agreement. We consider in more detail the results of DNS. The beginning of the interaction region ($X \approx 80$ mm) is characterized by a sharp decrease in skin friction and an increase in pressure. At $X \approx 97$ mm, backflow (negative wall-shear stress) begins to form due to laminar flow separation. In

the vicinity of the point with the coordinate $X \approx 111$–113 mm, there is a sharp increase in pressure induced by the main incident shock. The high positive pressure gradient leads to a sharp increase in the skin friction modulus in the backflow near the wall. Significant development of the separation flow downstream does not occur due to transition to turbulence in the shear layer. Laminar–turbulent transition occurs in a narrow region ($X \approx 112$–120 mm), resulting in a significant increase in the skin friction coefficient. As a result, a narrow peak of negative values of C_f is observed in the zone of intersection of the incident shock wave with the plate surface (see Fig. 3a). In the DNS simulation, the distribution of parameters show some oscillations in the wake region due to the insufficient averaging time.

The position and magnitude of the peak negative value of C_f determined using the ($\varkappa$–ω–γ–Re_θ) model in the RANS calculation agree well with the DNS results. This implies that this semi-empirical model predicts the initial process of transition to turbulence with sufficient accuracy. However, the data on the dimensions of the interaction zone and the separation zone and the wake flow parameters differ from the results of DNS. The dimensions of the interaction region obtained for the ($\varkappa_L$–$\varkappa_T$–ω) model coincide with the DNS results, but the transition to turbulence for the ($\varkappa_L$–$\varkappa_T$–ω) model occurs more slowly, which manifests itself in the smearing of the peak negative value of C_f and in a decrease in skin friction in the wake. When using the three-parameter ($\varkappa$–ω–γ) model, the results are close to the results obtained for the four-parameter ($\varkappa$–ω–γ–Re_θ) turbulence model. The ($\varkappa$–ω–γ) model provides results that are better consistent with the DNS results in the wake region, but at the beginning of the transition region, the results diverge (in the region of the peak negative value of C_f).

For the data obtained using the ($\varkappa$–ω)-SST model upstream of the point $X_t = 111$ mm, the turbulent viscosity was assumed to be zero. In this case, the dimensions of the separation zone and the values of C_f in the transition region obtained for the ($\varkappa$–ω)-SST model differ as much as possible from the data obtained by direct numerical simulation and the wake flow parameters are in good agreement.

Figure 4 shows the effect of the freestream flow turbulence intensity I_t on the skin friction coefficient in the case of RANS simulation using the ($\varkappa$–ω–γ–Re_θ) model. With increasing turbulence intensity from 0.01 to 1%, the length of the laminar bubble decreases almost twofold. In this case, the peak negative value of C_f increases and moves upstream. The change in the level of initial disturbances in the DNS should also lead to a change in the dimensions of the interaction region and the flow parameters in this region. Since in the DNS, the fluctuation level is directly specified for one unstable mode, and RANS simulations use an integral parameter, it is impossible to make a comparison under similar conditions. Nevertheless, for close levels of fluctuations of the incoming flow, the DNS and RANS data in Fig. 2 are in good agreement.

Analysis of the results of DNS and RANS simulations suggests that the turbulence models considered in this work taking into account laminar–turbulent transition can be used to obtain quantitative data on this type of flow. Basically, the differences are not significant, and the largest differences occur when using the ($\varkappa_L$–$\varkappa_T$–ω)-model.

We consider the reasons for the difference between the results of the experiment and numerical simulation. Figure 5 shows the longitudinal distributions of the displacement thickness. This quantity was calculated according to the formula for incompressible flow, since the experimental data on densities are absent. As noted above, the displacement thickness in the laminar bubble and in the wake region increases more significantly in the experiment than in the DNS and RANS simulations. This may be due to the features of the wake flow simulation, where all the calculation methods underestimate the value of the displacement thickness. In this case, the freestream Mach number is small (M = 1.43), and the wake Mach number behind the system of shock and rarefaction waves is close to unity; thus, in the shear layer, large subsonic regions appear, through which the upstream flow is affected. The interaction of the shock wave with the boundary layer is practically identical to their interaction in the case of transonic flow, where even small changes in individual parameters can lead to flow restructuring as a whole [23]. In direct numerical simulations, in addition to the insufficient resolution of turbulent structures in the wake, it is necessary to take into account that the laminar–turbulent transition is caused by the development of one unstable disturbance mode. Since in the problem under consideration, laminar–turbulent transition occurs rather rapidly (at a distance of about eight local displacement thicknesses), it can be assumed that the nonlinear development of disturbances depends largely on the spectral composition and amplitudes of disturbances. As a result, the wake flow can change significantly with changing initial level of disturbances in DNS simulations. This is partially supported by experimental studies [24], where the measured boundary layer thickness in the wake region behind the interaction zone in the case of a laminar incoming layer is significantly larger than in the case where the state of the incoming

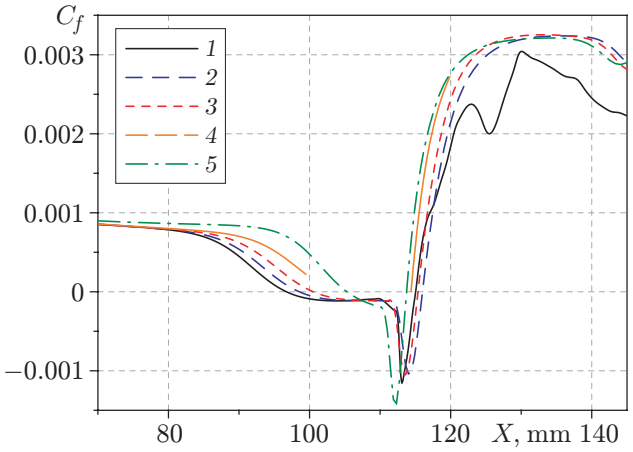

Fig. 4.

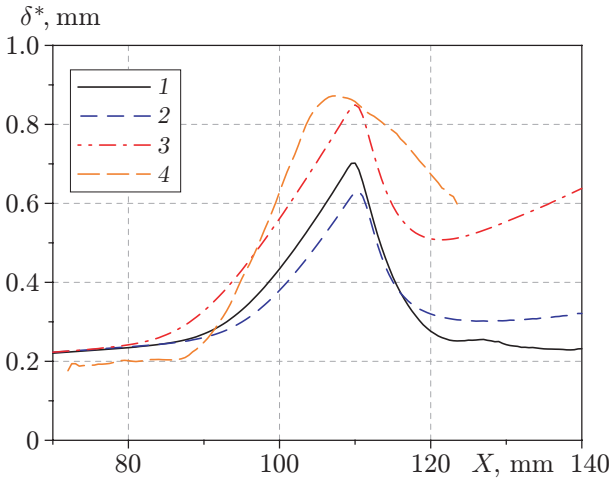

Fig. 5.

Fig. 4. Skin friction distributions along the longitudinal coordinate obtained by DNS simulation (*1*) and RANS simulation for $I_t = 0.01$ (*2*), 0.1 (*3*), 0.5 (*4*), and 1% (*5*).

Fig. 5. Displacement thickness distributions obtained by DNS simulation (*1*) and RANS simulation for the ($\varkappa$–ω–γ–Re_θ) model (*2*) and the modified ($\varkappa$–ω–γ–Re_θ) model (*3*); curve *4* refers to the experimental data.

boundary layer corresponded to the beginning of the transition process. To confirm this assumption, it is necessary to perform DNS simulations for different frequencies of incoming disturbances.

In the transitional turbulence models used in RANS simulations, there is no opportunity to change the spectral composition of incoming disturbances; therefore, to solve this problem, it is necessary to make corrections to the equations of turbulence kinetic energy transfer. Figure 5 shows the results obtained using various models, including a modified ($\varkappa$–ω–γ–Re_θ) model in which the additional dissipative term $\varkappa$ for the wake region is introduced in the convection equation. It can be seen that when using the modified equation, the simulation data are in much better agreement with the experimental results. Note that the dissipative term affects the flow only after the flow transition to turbulence; therefore, the increase in the displacement thickness in the laminar bubble region is caused precisely by the change in the flow pattern in the wake. The large displacement thickness in the wake leads to a change in pressure distribution, resulting in a change in the flow pattern in the separation zone. These data indicate the need for correct calculation of the region behind the interaction zone, whose development, in turn, depends on the processes of laminar–turbulent transition.

Linear stability theory and the e^N method are often used to predict laminar–turbulent transition in solving practical problems. Therefore, it is important to evaluate the possibility of using the locally parallel LST theory for this flow, where in the interaction zone and in the separation bubble, there is a rather rapid change in the parameters along the longitudinal coordinate.

Figure 6 shows a spectrogram of pressure fluctuations on the wall of the plate P_{SD} obtained from the DNS results. It is seen that ahead of the interaction region, there is one frequency corresponding to the introduced disturbance. At the beginning of the interaction region, the amplitude of disturbances increases over a wide frequency range. The presence of a wide range of frequencies in the beginning of the interaction region is obviously due to the development of natural disturbances in the separation region, which should not affect the development of the unstable mode. Thus, it can be assumed that the disturbance develops linearly in the region up to the point of intersection of the incident shock wave with the plate. At the point of the beginning of the pressure plateau ($X \approx 100$ mm), which corresponds to flow separation, there is a local damping of all fluctuations of the spectrum, except for the unstable mode. Downstream, near the point of intersection of the incident shock with the plate, the amplitude of disturbances increases significantly and the spectrum is filled with harmonics of the introduced mode. Nonlinear processes develop at high rate, which leads to the occurrence of turbulent flow.

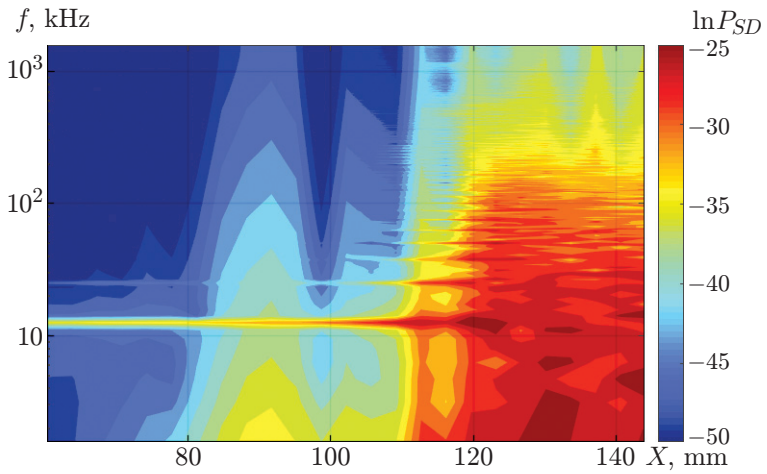

Fig. 6. Spectrogram of pressure fluctuations on the wall obtained by DNS simulation.

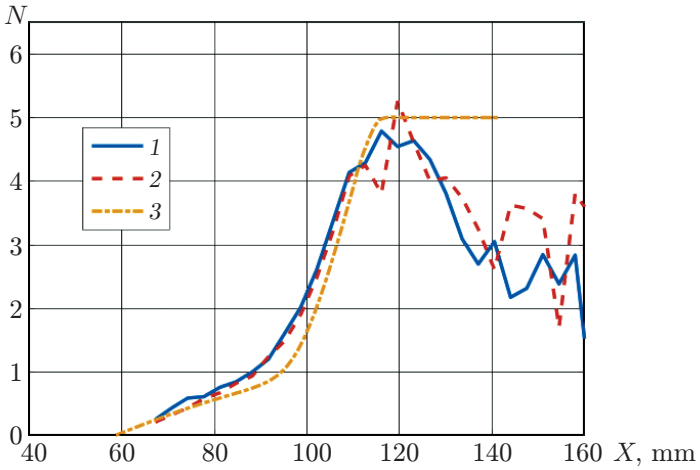

Fig. 7. Distributions of N-factors: curve *1* refers to the results of DNS simulation using the wall pressure, curve *2* to the results of DNS simulation using the skin friction, and curve *3* to the results of LST simulation using the growth rate.

Figure 7 shows the distributions of N-factors of growing disturbances obtained by DNS and LST simulations using LOTRAN code [25]. Time-averaged boundary-layer profiles obtained by DNS simulation were used as the mean flow in stability calculations. It is seen that in the DNS simulation, the data obtained by analyzing fluctuations of the pressure (curve *1*) and the skin friction (curve *2*) ahead of the region of the transition to turbulence in the boundary layer are in good agreement. The growth rates (curve *3* in Fig. 7) were obtained using linear theory for the disturbance corresponding to the initial disturbance in the DNS ($f = 25.1$ kHz and $\chi = 46°$). It can be seen that the data obtained in the LST and DNS calculations are in good agreement. Furthermore, one can see a significant increase in the amplitude of disturbances in the region of the laminar separation bubble and a gradual increase in the amplitude of disturbances in the incoming boundary layer. Thus, the data indicate the possibility of using the e^N method in the region of the laminar separation bubble for the problem under study.

CONCLUSIONS

Numerical simulation of the flow in the region of interaction of a shock wave with a laminar boundary layer for a Mach number M = 1.43 was performed. The results obtained using RANS methods taking into account laminar–turbulent transition agree well with the data of direct numerical simulation. The results show that existing RANS models are suitable for calculating compressible laminar separation flows, at least in the case of a high unfavorable pressure gradient.

It is shown that the DNS and LST methods provide consistent predictions of the growth in the amplitude of disturbances in the boundary layer and in the laminar separation bubble. This suggests that locally parallel stability theory and the e^N method are suitable for determining the position of the transition for the investigated class of problems.

Differences between the experimental and calculated data are found mainly in the region of flow transition to turbulence and in the turbulent wake and require further research using both approaches. These differences may be due to nonlinear effects in the zone of transition to turbulence, leading to significant non-equilibrium of the turbulent boundary layer in the wake behind the separation zone.

This work was supported by the Russian Science Foundation (Project No. 18-19-00547).

REFERENCES

1. J. Green, "Interactions between Shock Waves and Turbulent Boundary Layers," Progr. Aerospace Sci. **11**, 235–340 (1970).
2. D. S. Dolling, "Fifty Years of Shock Wave/Boundary Layer Interaction: What Next," AIAA J. **39**, 1517–1531 (2001).
3. A. J. Smits, *Turbulent Shear Layers in Supersonic Flow,* Ed. by A. J. Smits and J. P. Dussauge (Woodbury, New York, 1996).
4. A. Zheltovodov, "Shock Wave/Turbulent Boundary Layer Interactions: Fundamental Studies and Applications," AIAA Paper No. 1996-1977 (New Orleans, 1996).
5. Y. Andreopoulos, J. H. Agui, and G. Briassulis, "Shock Wave–Turbulence Interactions," Annual Rev. Fluid Mech. **32**, 309–345 (2000).
6. H. Babinsky, *Shock Wave–Boundary-Layer Interactions*, Ed. by H. Babinsky and J. K. Harvey (Cambridge Univ. Press, 2011).
7. *Unsteady Effects of Shock Wave Induced Separation*, Ed. by P. Doerffer, C. Hirsch, J.-P. Dussauge, et al. (Springer, 2011). (Notes Numer. Fluid Mech. Multidisciplinary Design; Vol. 114.)
8. N. T. Clemens and V. Narayanaswamy, "Low-Frequency Unsteadiness of Shock Wave/Turbulent Boundary Layer Interactions," Annual Rev. Fluid Mech. **46**, 469–492 (2014).
9. D. Di Pasquale, A. Rona, and S. Garrett, "A Selective Review of Transition Modeling for CFDs," (AIAA Paper No. 2009-3812) (San Antonio, 2009).
10. D. Knight and G. Degrez, "Shock Wave Boundary Layer Interactions in High Mach Number Flows: A Critical Survey of Current CFD Prediction Capabilities," Tech. Report No. AR-319-02 (Advisory Group for Aerospace Research and Development, Neuilly-sur-Seine, 1998).
11. S. Teramoto, "Large-Eddy Simulation of Transitional Boundary Layer with Impinging Shock Wave," AIAA J. **43** (11), 2354–2363 (2005).
12. E. Touber and N. D. Sandham, "Large-Eddy Simulation of Low-Frequency Unsteadiness in a Turbulent Shock-Induced Separation Bubble," Theor. Comput. Fluid Dyn. **23**, 79–107 (2009).
13. E. Garnier, P. Sagaut, and M. O. Deville, "Large Eddy Simulation of Shock/Boundary Layer Interaction," AIAA J. **40** (10), 1935–1944 (2002).
14. S. Pirozzoli and F. Grasso, "Direct Numerical Simulation of Impinging Shock Wave/Turbulent Boundary Layer Interaction at M = 2.25," Phys. Fluids **18** (6), 065113 (2007).
15. M. Wu and P. Martin, "Direct Numerical Simulation of Supersonic Turbulent Voundary Layer over a Compression Ramp," AIAA J. **45** (4), 879–889 (2007).
16. C. Mayer, D. von Terzi, and H. Fasel, "Direct Numerical Simulation of Complete Transition to Turbulence via Oblique Breakdown at Mach 3," J. Fluid Mech. **674**, 5–42 (2011).

17. I. V. Egorov, A. V. Novikov, and A. V. Fedorov, "Direct Numerical Simulation of the Laminar–Turbulent Transition at Hypersonic Flow Velocities on a Supercomputer," Zh. Vychsil. Mat. Mat. Fiz. **57** (8), 1347–1373 (2017) [Comput. Math. Math. Phys. **57**, 1335–1359 (2017); https://doi.org/10.1134/S0965542517080061].
18. A. N. Kudryavtsev and D. V. Khotyanovsky, "Direct Numerical Simulation of Transition to Turbulence in a Supersonic Boundary Layer," Teplofiz. Aeromekh. **22** (5), 581–590 (2015) [Thermophys. Aeromech. **22** (5), 559–568 (2015); https://doi.org/10.1134/S0869864315050042].
19. D. V. Khotyanovsky and A. N. Kudryavtsev, "Numerical Simulation of the Evolution of Unstable Disturbances of Various Modes and Initial Stages of the Laminar–Turbulent Transition in the Boundary Layer at the Freestream Mach Number M = 6," Teplofiz. Aeromekh. **23** (6), 843–852 (2016) [Thermophys. Aeromech. **23** (6) 809–818 (2016); https://doi.org/10.1134/S0869864316060032].
20. P. A. Polivanov, A. A. Sidorenko, and A. A. Maslov, "Transition Effect on Shock Wave/Boundary Layer Interaction at M = 1.47," AIAA Paper No. 2015-1974 (Kissimmee, 2015).
21. P. A. Polivanov and A. A. Sidorenko, "Suppressing a Laminar Flow Separation Zone by Spark Discharge at Mach Number M = 1.43," Pis'ma Zh. Tekh. Fiz. **44** (18), 60–68 (2018) [Tech. Phys. Lett. **44**, 833–836 (2018); https://doi.org/10.1134/S1063785018090262].
22. P. A. Polivanov, A. A. Sidorenko, and A. A. Maslov, "The Influence of the Laminar–Turbulent Transition on the Interaction between the Shock Wave and Boundary Layer at a Low Supersonic Mach Number," Pis'ma Zh. Tekh. Fiz. **41** (19), 29–37 (2015) [Tech. Phys. Lett. **41**, 933–937 (2015); https://doi.org/10.1134/S1063785015100120].
23. A. I. Kutepova, P. A. Polivanov, and A. A. Sidorenko, "Effect of a Uncertainties of Flow Parameters on the Separation Zone at Supersonic Speeds," J. Phys.: Conf. Ser. **1404**, 012085 (2019); DOI: 10.1088/1742-6596/1404/1/012085.
24. P. A. Polivanov, A. A. Sidorenko, and A. A. Maslov, "Study of the Unsteady Structures Evolution in Shock Wave/Boundary Layer Interaction for Various Upstream Conditions," in *Proc. of the 30th Congr. of the Int. Council of the Aeronautical Science (ICAS 2016), Daejeon, Korea, September 25–30, 2016*, pp. 1–10.
25. A. V. Boiko, K. V. Demyanko, A. A. Inozemtsev, et al., "Determination of the Laminar–Turbulent Transition Location in Numerical Simulations of Subsonic and Transonic Flows Past a Flat Plate," Teplofiz. Aeromekh. **26** (5), 675–683 (2019) [Thermophys. Aeromech. **26** (5), 629–637 (2019); https://doi.org/10.1134/S0869864319050019].